Thermodynamic stability of transition metals on the Mg-terminated MgB_2 (0001) surface and their effects on hydrogen dissociation and diffusion

Yongli Wang, Kyle Michel, Yongsheng Zhang, and C. Wolverton
Department of Materials Science and Engineering, Northwestern University, Evanston, Illinois 60208, USA
(Received 24 June 2014; revised manuscript received 8 April 2015; published 27 April 2015)

The hydrogenation of MgB_2 is a critical step in the reversibility of several well-known hydrogen storage reactions. Of the many processes that must occur during rehydrogenation, at least two of them take place near the surface: the dissociation of H_2 molecules and the subsequent diffusion of atomic hydrogen. Using first-principles calculations, we determine the energetic barriers for these processes on the ideal Mg-terminated MgB_2 (0001) surface, as well as on surfaces containing transition metal dopants (Sc-Zn, Y-Cd, Pt, and Au). The calculated dissociation barrier for H_2 on the clean surface is 0.89 eV, and the surface diffusion barrier is 0.17 eV. However, we find examples of dopants that significantly decrease the activation barrier for the dissociation of H_2. Our calculations suggest that Ni, Cu, and Pd are good catalytic candidates for the surface processes involved in MgB_2 rehydrogenation.

DOI: 10.1103/PhysRevB.91.155431 PACS number(s): 68.43.Bc, 82.65.+r, 73.20.Hb

I. INTRODUCTION

The design of safe, efficient, and economical hydrogen storage materials is a crucial barrier to the utilization of hydrogen as a fuel source for passenger vehicles. Complex metal hydrides have long been investigated as possible hydrogen storage materials because of their high volumetric and gravimetric densities [1–5]. Candidate complex metal hydrides as storage material also should have desired thermodynamics that allow the release of H_2 at a few bar using the waste heat from the proton exchange membrane fuel cell [6,7]. In addition to re/dehydrogenation in the targeted range of temperatures and pressures, the re/dehydrogenation processes should take place rapidly. The Department of Energy has a target for the rehydrogenation rate of 2.0 kg H_2/min and has also established targets for many other properties (such as operational cycle life) [8]. However, no material has been found that simultaneously meets the thermodynamic, kinetic, and other requirements for practical, on-board hydrogen storage materials.

The demonstration that catalyzed $NaAlH_4$ has a low hydrogen release temperature (around 100 °C) as well as reversibility [9] triggered extensive research on hydrogen release and decomposition pathways of complex metal hydrides [3,10–12]. In particular, two complex hydride systems attracted intense interest: (1) The first involves $Mg(BH_4)_2$, which contains 14.9% hydrogen by weight [13] and has promising thermodynamics properties that distinguish it from other metal borohydrides [14–16]. Previous experimental and theoretical studies found that the first step of $Mg(BH_4)_2$ decomposition has a high gravimetric storage capacity (8.1 wt. %) and a reaction enthalpy of about 40 kJ/(mol H_2) [$Mg(BH_4)_2$ -> $1/6MgB_{12}H_{12} + 5/6MgH_2 + 13/6H_2$ -> $MgB_2 + 4H_2$], which is within the targeted range of enthalpies for near-ambient desorption [17–22]. In addition, Severa *et al.* [23] successfully rehydrogenated commercially available MgB_2 under 95 MPa hydrogen pressure and 400 °C to obtain $Mg(BH_4)_2$, which presented the possibility of full reversibility in $Mg(BH_4)_2$. (2) The other system of interest is the mixture of $LiBH_4$ and MgH_2 ($MgH_2 + 2LiBH_4$ -> $MgB_2 + 2LiH + 4H_2$). The $TiCl_3$ doped mixture of $MgH_2 + 2\,LiBH_4$ (or the decomposition products $MgB_2 + 2\,LiH$) was found to have a reversible storage of 8–10 wt. % H_2, but a long equilibrium time, around 100 h at 300–350 °C [24,25]. Albeit the advantages in thermodynamics and reversibility, neither of the two systems has a fast desorption or adsorption rate that is suitable for mobile applications.

The end product of these two well-known systems is MgB_2, whose hydrogenation is a critical step for the reversibility and also influence the kinetic reaction rates. Therefore, a solid understanding of MgB_2 hydrogenation mechanisms can assist to identify the rate limiting steps, and potentially provide new paths to tackle the kinetic constraints and boost reaction rates. Prior experimental efforts have been devoted to improve the reversibility and reaction rates of complex hydride and demonstrated that transition metals can dramatically enable much lower H_2 release temperature and fast desorption rate. In particular, Newhouse *et al.* [26] found that the addition of 5 mol % of $ScCl_3$ and TiF_3 to $Mg(BH_4)_2$ improved the hydrogen desorption capacity and kinetics, with MgB_2 as an end product at 600 °C. Compared with the sample without Sc or Ti additives, after the rehydrogenation reaction, less residual MgB_2 was detected, suggesting the additives aid the rehydrogenation process. However, these additives produced less $Mg(BH_4)_2$ but more $MgB_{12}H_{12}$ (Ref. [26], Table 2).

The hydrogenation of MgB_2 has not been extensively explored and the mechanism of transition metals for H_2 adsorption is still not completely understood. Many processes could impair the kinetic rates, such as nucleation, defect diffusion, and H_2 dissociation and diffusion at surfaces. Previous theoretical studies demonstrated that computational methods can be applied in the study of kinetic process for various hydrogen storage systems [27–37], and some systems (such as AlH_3 and MgH_2) were reported to have undesired H_2 dissociation barriers which may hinder the reaction process [27–30,38–40]. Thus, as an initial stage to examine the kinetic process for MgB_2 hydrogenation and find out the possible rate limiting processes, we studied hydrogen dissociation and diffusion on MgB_2 surface in this work (and

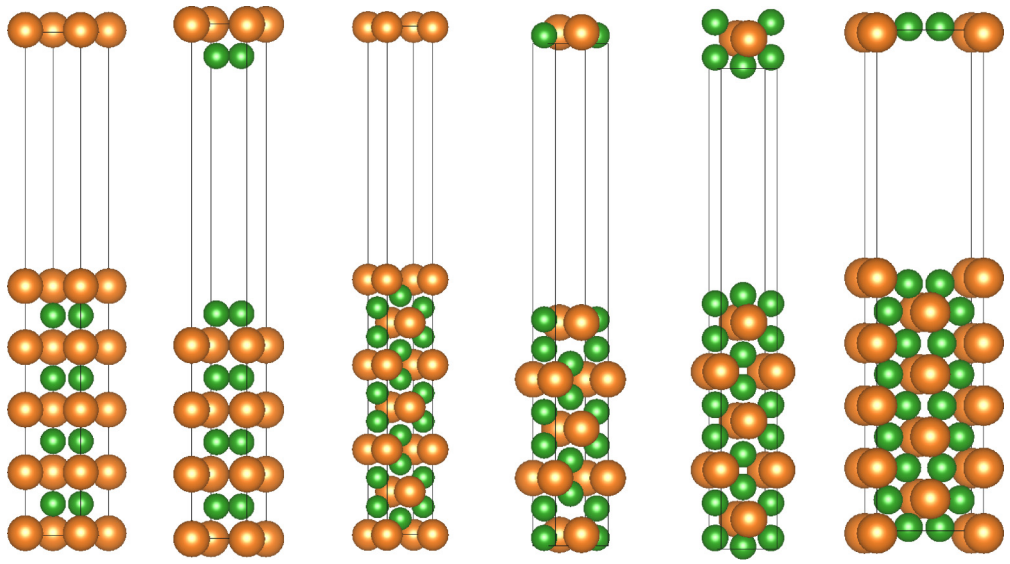

FIG. 1. (Color online) We illustrate the DFT-relaxed surface structure of Mg-terminated (0001), B-terminated (0001), Mg-terminated (10$\bar{1}$0), two kinds of B-terminated (10$\bar{1}$0), and Mg-B-terminated (11$\bar{2}$0), from left to right, respectively. The first kind of B-terminated (10$\bar{1}$0) surface, annotated as (10$\bar{1}$0)-B1 in Table I, is terminated by boron layer, but with Mg layer as the subsurface layer. The other B-terminated (10$\bar{1}$0) surface, annotated as (10$\bar{1}$0)-B2 in Table I, has another boron layer as the subsurface layer. All surfaces cells are 1×1 in the surface plane, except for the (11$\bar{2}$0) surface, which is 2×1. The bigger (orange) atoms represent Mg atoms, while the smaller (green) ones represent B atoms.

hydrogen diffusion in bulk MgB_2 in a separate paper [41]). We also present the analysis of the effects of transition metals on the surface hydrogen dissociation and diffusion.

In the current work we utilized first-principle methods to explore the hydrogen adsorption, dissociation, and diffusion behaviors on the clean and transition metal doped MgB_2 surface. We identified a high dissociation barrier and a low surface diffusion barrier. In addition, we report the catalytic effects of various TM additions depending on the position of the additives in the periodic table through a systematic examination of the 3*d* and 4*d* transition metal dopants. We find the majority of transition metals can reduce the dissociation barrier but simultaneously increase the surface diffusion barrier, especially for early transition metal additives. Among the studied dopants, we show that Ni, Cu, and Pd, and to some extent V, Cr, Mn, Fe, and Co can reduce the H_2 dissociation barrier without impairing surface diffusion, and can potentially accelerate MgB_2 hydrogen adsorption rate. As a final note, we hope that our first-principles results will stimulate experimental evaluation of these complex hydrides and tests of our predictions.

II. COMPUTATIONAL METHOD

To investigate the kinetic behavior of hydrogen on the MgB_2 surfaces, we use first-principles density functional theory (DFT) ($T = 0$ K) [42,43] to compute surface energies, hydrogen binding energies, and substitutional energies of transition metals on the surfaces. In order to determine which surfaces have low energies, and hence will likely be the most prevalent, we must calculate the surface energies of many surfaces. To estimate the relative thermodynamic stability of different MgB_2 surfaces, we calculate the surface energy $E_{\rm surf}$ of several low index B, Mg, and B-Mg terminations. The surface energy per unit area $E_{\rm surf}$ can be written as

$$E_{\rm surf} = \frac{E_{\rm slab}^{\rm MgB_2} - N_{\rm atoms} E_{\rm bulk}^{\rm MgB_2} - \sum_i n_i \mu_i}{2A}, \qquad (1)$$

which is the total energy difference per unit area of surface between the slab of MgB_2 and the bulk of MgB_2, as well as the chemical potential of B and Mg. $E_{\rm slab}^{\rm MgB_2}$ is the total energy of the MgB_2 slab, and $N_{\rm atoms}$ corresponds to the number of atoms in the MgB_2 slab. n_i indicates the number of nonstoichiometric atoms of type i that arise from creating the surface. For example, in order to generate a Mg-terminated (0001) surface, one extra Mg atom per 1×1 unit cell needs to be put in the MgB_2 slabs. That is, $n_{\rm Mg} = 1$ and $n_B = 0$ for a 1×1 unit cell of Mg-terminated (0001) surface [Fig. 1(a)]. μ_i are the corresponding chemical potentials of Mg and B species. Further discussion about the calculation of $\mu_{\rm Mg}$ and $\mu_{\rm B}$ can be found in Sec. III A. A is the area of the surface.

To study the dissociation and diffusion of hydrogen on the low energy MgB_2 surfaces, we need to obtain the adsorbed atomic hydrogen binding energies and determine the stable hydrogen adsorption sites and patterns. The average binding energy of the adsorbed atomic hydrogen can be expressed as

$$E_b(\theta) = \frac{1}{N \times \theta}\left[E_{\rm slab}^{\rm H/MgB_2}(\theta) - E_{\rm slab}^{\rm MgB_2} - \frac{N \times \theta}{2} E_{\rm H_2}\right], \qquad (2)$$

where θ is the adsorbed hydrogen atom coverage ratio. It is defined as the ratio of the number of adsorbed hydrogen atoms to the number of Mg atoms in an ideal Mg surface layer. N is the number of primitive cells that are contained in the

calculated supercell. E_{slab}^{H/MgB_2} and $E_{slab}^{MgB_2}$ are the total DFT energies of the slabs with and without adsorbed hydrogen atoms. E_{H_2} is the total energy of a free hydrogen molecule, obtained by relaxing a hydrogen molecule in a fixed $10 \times 10 \times 11$ Å^3 box. According to Eq. (2), a negative hydrogen binding energy means the chemisorbed hydrogen is stable, while a positive value indicates that it is energetically more favorable for hydrogen to be in the gas phase.

In order to probe the dopant effects on rehydrogenation, we must first compute the substitutional energies of dopants on surface sites. The substitutional energy (E_{sub}) of transition metals on MgB_2 surfaces is defined as

$$E_{sub} = E_{slab}^{TM/MgB_2} + \mu_{Mg} - \mu_{TM} - E_{slab}^{MgB_2}, \quad (3)$$

where E_{slab}^{TM/MgB_2} is the total DFT energy of the transition metal substituted on the MgB_2 surface, and μ_{Mg} and μ_{TM} are the chemical potentials for Mg and the transition metal, respectively. Further discussion about the calculation of TM chemical potentials can be found in Sec. III A. $E_{slab}^{MgB_2}$ is the total DFT energy of the clean (without doping or hydrogen) MgB_2 slabs.

To obtain the total energies of ideal surfaces, hydrogen adsorbed surfaces, and TM-doped surfaces, first-principles density functional theory [42,43] calculations were performed using the Vienna *ab initio* simulation package (VASP) [44] with the Perdew-Wang (PW91) generalized gradient approximation [45] and Blöchl's projector augmented wave (PAW) method [46,47]. In all of our calculations, the plane-wave cutoff energy was set at 450 eV. Surfaces are modeled by periodic slabs separated by a vacuum region of 15 Å. In each surface slab, at least three MgB_2 layers are used, with the bottom two MgB_2 layers fixed at the bulk positions. Atomistic relaxations of the hydrogen adsorbed surface were performed using cell sizes of 1×1, 2×2, and 3×3 surface periodicities. Hydrogen dissociation and diffusion are studied in a 2×2 unit cell. The k-space integrals are evaluated using a 4×4 grid for the 2×2 unit cell. The convergence for electronic structure optimization was set to 10^{-5} eV while the atomic coordinates were refined until all forces were below 10^{-2} eV/Å. Spin polarization calculations were performed for the magnetic transition metals.

After determining the low energy surfaces, stable atomic hydrogen adsorption pattern, and substitutional energies of transition metals, we moved on to study the dissociation and diffusion of hydrogen on the surfaces. Dissociation and diffusion paths were found using the nudged elastic band (NEB) method [48], and climbing image NEB [49] calculations were preformed to find the barriers. In the NEB calculations, starting guesses for the intermediate structures were generated by interpolating images between the DFT relaxed initial and final states. In Sec. III we present the discussion of how we obtained the initial and final states. Once these paths had been explored, the transition state for each was further refined using the climbing image nudged elastic band method [50]. The dissociation and migration energy (Table II) was defined as the total energy difference between the initial and transition states.

III. RESULTS AND DISCUSSION

A. Stability of MgB_2 surfaces

We begin by investigating the stability of MgB_2 surfaces. The bulk structure of MgB_2 we use in the study of MgB_2 surfaces has a hexagonal symmetry (space group: $P6/mm$) [41,51], formed by alternating hexagonal Mg layers and honeycomb B layers, stacked along [0001] direction. We search for low-energy surfaces and use those surfaces to explore the reaction with hydrogen molecule/atoms. Unfortunately, there are no clear experimental results that identify which surfaces of MgB_2 interact with H_2 during hydrogenation. The chemical potentials that appear in Eq. (1) account for the energy of Mg and B atoms that are added or removed in nonstoichiometric surfaces. While these chemical potentials are determined by the experimental conditions, bounds can be placed on the Mg and B chemical potentials by considering stability of MgB_2 with Mg-rich and B-rich phases on the Mg-B binary phase diagram. Based on the Open Quantum Materials Database (OQMD) [52], the Mg-rich and B-rich equilibrium phases with MgB_2 on the Mg-B binary phase diagram are identified as Mg and MgB_4, respectively. μ_{Mg} and μ_B can be expressed in terms of a linear combination of the energies of these two set phases (i.e., $MgB_2 + MgB_4$ and $MgB_2 + Mg$). A detailed example on calculation of chemical potentials is given in Sec. III C. For each surface we show the surface energy under each of these two sets of chemical potentials, which place bounds on the surface energies that could exist. From Table I we can see that the lowest energy surface is the Mg-terminated (0001) surface, which indicates that it will be the most prevalent surface in equilibrium samples. This result can be understood, since with hexagonal symmetry a cut along the basal plane of MgB_2 breaks the fewest bonds to form the surface, and the Mg surface energy is lower than B. As a final note, MgB_2 is a well-known superconductor, and Mg-terminated (0001) surface has been identified and studied for the investigation of MgB_2 superconductivity [53–56]. No surface reconstruction has been observed in the previous works [53–56]. Therefore, this study also focus on the unreconstructed ideal surface. In the following discussion, we study the interaction of hydrogen on the Mg-terminated (0001) surface.

B. Hydrogen adsorption on the Mg-terminated (0001) surface of MgB_2

The [0001] direction of MgB_2 is composed of alternating boron honeycomb layers and Mg hexagonal layers. The top view of the Mg-terminated surface is shown in Fig. 2. Figure 2 also shows the three high symmetry sites (top, bridge, and hollow) that were selected as possible adatom sites. Three calculations were performed, with the atomic hydrogen put on the top, bridge, and hollow sites of a 2×2 unit cell surface, each in a separate calculation. It is found that the hollow site is the lowest-energy site for adsorption of atomic hydrogen. In fact, only the hollow site is stable while there is a barrierless path to it from the top and bridge sites.

To explore the interaction between atomic hydrogen and the Mg-terminated MgB_2 (0001) surface, the hydrogen surface

TABLE I. DFT calculated surface energies as defined in Eq. (1). We calculated several low surface indexes, terminated with different species (Mg, B, or both). The surface structures are shown in Fig. 1. The column of (n_{Mg}, n_B) shows how many extra Mg, B chemical potentials need to be removed from the total surface energy to obtain the surface energy. Two sets of chemical potentials are considered, which provide bounds for the surface energies. One set is determined by assuming equilibrium between MgB_2 + Mg, and the other is determined by equilibrium between MgB_2 + MgB_4. The (0001) Mg-terminated surface is the lowest energy, regardless of chemical potentials. Figure 1 introduces the "B1" and "B2" notation.

				ΔE_f (J/m^2)	
Index	Termination	Surface area (Å^2)	(n_{Mg}, n_B)	MgB_2 + Mg equilibrium	MgB_2 + MgB_4 equilibrium
(0001)	Mg	8.17	(1,0)	0.82	0.92
(0001)	B	8.17	(0,2)	2.89	2.79
(10$\bar{1}$0)	Mg	10.84	(1,0)	1.32	1.40
(10$\bar{1}$0)	B1	10.84	(0,0)	3.83	3.83
(10$\bar{1}$0)	B2	10.84	(0,2)	2.64	2.58
(11$\bar{2}$0)	Mg-B	18.78	(0,0)	2.28	2.28

binding energy [Eq. (2)] was computed under different coverage ratios. Due to a partial charge transfer from the surface to the hydrogen atom, there is a dipole moment associated with each. Normally the dipole-dipole interaction is repulsive, leading to less favorable binding energies for increasing coverage [57,58]. However, as shown in Fig. 3, the behavior of the hydrogen surface binding energy is more complex than that. In the coverage regime $0 < \theta < 1$ ML, one can see from Fig. 3 that the binding energy becomes more favorable with increasing hydrogen coverage. We also calculated the energies of many different adatom configurations for each coverage ratio. The lowest energy configuration for coverages $\theta = 0.5$ ML and $\theta = 0.75$ ML are shown in Fig. 4, and typically increase by up to 60 meV/(H atom) in the least favorable configurations. From these calculations of various adsorbed H configurations, we can deduce some simple rules about favorable adsorption patterns. The main finding is that the adsorbed H tends to maximize its distance from other adsorbed H. Comparing Figs. 4(c) and 4(d), it is obvious that there is a strong repulsion between nearest neighbor hydrogen if they are adsorbed in the two nearest neighbor hollow sites. This observation is also true for $\theta = 0.5$ ML. The lowest energy configuration for $\theta = 0.5$ ML [Fig. 4(a)] has an average hydrogen distance of 4.2 Å compared with 3.5 Å for configuration of Fig. 4(b) [the latter is the average of H-H distances of 3.1 and 5.3 Å, see Fig. 4(b)]. Moreover, the lowest configuration of 0.25, 0.5, 0.7, and 1 ML [Figs. 4(e), 4(a), 4(c), and 4(f)] share a similar adsorption pattern. Without changing the 0.75 ML lowest-energy configuration, the lowest-energy configuration for 1 ML is just to adsorb one more hydrogen on the hollow site which is as far as possible from other hydrogen adsorption sites. This behavior can also be seen by comparing low energy configurations at 0.25 and 0.5 ML, and also comparing 0.5

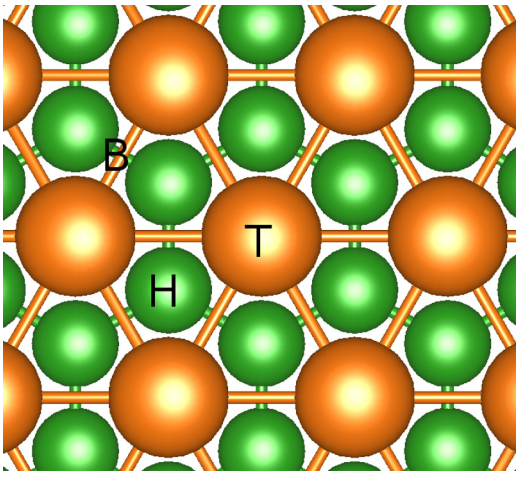

FIG. 2. (Color online) Three different high symmetry sites for hydrogen adsorption on the Mg-terminated (0001) MgB_2 surface (top view). "T," "B," and "H" denote the top, bridge, and hollow sites, respectively. It is unstable for hydrogen to be adsorbed on the top and bridge sites. The system will be at the local minimum energy if hydrogen stays at hollow site. The bigger (orange) atoms represent Mg atoms, while the smaller (green) ones represent B atoms.

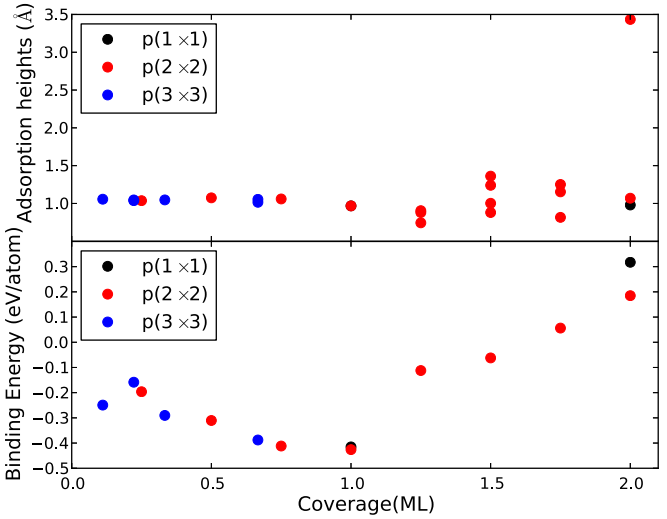

FIG. 3. (Color online) Calculated hydrogen binding energy vs different coverage ratios on the Mg-terminated MgB_2 (0001) surface. The binding energy is defined in Eq. (2). A negative binding energy indicates that the hydrogen adsorption is stable. The black, red, and blue dots represent hydrogen adsorbed on 1 × 1, 2 × 2, and 3 × 3 surface unit cells, respectively.

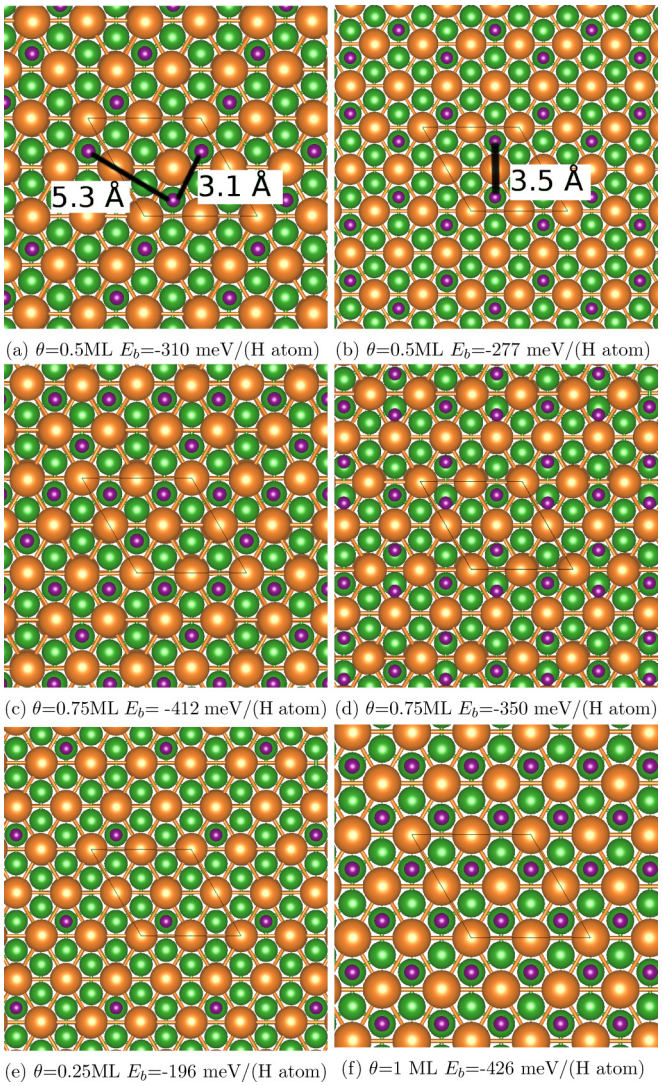

(a) θ=0.5ML E_b=-310 meV/(H atom) (b) θ=0.5ML E_b=-277 meV/(H atom)

(c) θ=0.75ML E_b= -412 meV/(H atom) (d) θ=0.75ML E_b=-350 meV/(H atom)

(e) θ=0.25ML E_b=-196 meV/(H atom) (f) θ=1 ML E_b=-426 meV/(H atom)

FIG. 4. (Color online) Configurations for hydrogen at coverage ratio of 0.5, 0.75, 0.25, and 1 ML produced from the $p(2 \times 2)$ surface unit cell. E_b is the binding energy defined in Eq. (2). The purple, green, and orange atoms represent the H, B, and Mg species. We observe that the adsorbed atomic hydrogens generally try to maximize their distances from one another. Further discussion about hydrogen adsorption patterns can be found in Sec. III B.

and 0.7 ML. These lowest-energy configurations maximize the average distance between adsorbed hydrogens.

To study the hydrogen adsorption in the coverage range of $1 < \theta \leqslant 2$ ML, we choose a 2×2 supercell and construct four coverage ratios, i.e., $\theta = 1.25$, 1.5, 1.75, and 2 ML. Compared with a 1.0 Å relaxed distance away from the Mg layer for θ under 1 ML, for these high-coverage configurations, some of the H relaxes to a distance of 1.2 to 1.5 Å away from the surface Mg layer (Fig. 3). The binding energy also becomes less favorable with increasing hydrogen coverage for $1 < \theta \leqslant 2$ ML. Finally, we note that we did not consider temperature and pressure effects on binding energies or adsorption configurations.

To conclude this section on hydrogen surface adsorption, we summarize that the present calculations lead to the conclusion that atomic hydrogen adsorption on the Mg-terminated MgB_2 (0001) surface is stable for the coverage ratio of $0 < \theta \leqslant 1$ ML, and it becomes increasingly energetically unfavorable for hydrogen to be adsorbed at coverage ratios higher than 1 ML. The fully relaxed adsorbed atomic hydrogen for $0 < \theta \leqslant 1$ ML is around 1 Å above the Mg layer, with a Mg-H bond length of 2.05 Å, which is comparable with 1.98 Å of the Mg-H bond length in the bulk of MgH_2. As a final note, it is possible that surface stability will change with respect to adsorbates on the surface [59]. In this work we have focused on hydrogen interactions with the low-energy Mg-terminated (0001) surface. In the absence of adsorbates, this Mg-terminated (0001) surface is low in energy, and thus H_2 will initially interact with this surface.

C. Stability of TMs and vacancies on the MgB_2 (0001) surface

Having studied the tendency of hydrogen to form on the clean MgB_2 surface, we now turn to the investigation of this process on TM-doped surfaces. We first show the formation energies of the TMs substituting for atoms on the MgB_2 (0001) surface. As dopants, transition metals can substitute for Mg or B atoms. However, we find that substitution in the boron layer is extremely energetically unfavorable, and always has a very high formation energy. Therefore, we consider substitution only in the Mg layer for the remainder of this section.

The substitutional energy for transition metal doping in the MgB_2 surface is defined by Eq. (3), where the chemical potentials of Mg and transition metals must be specified and should be chosen to represent experimental conditions. The chemical potentials indicate the energy change of atoms to exchange between MgB_2 and their respective reservoirs. The reservoirs, in this work, should be the stable combination of phases formed when doping a small amount of TM for Mg in MgB_2. This combination of phases cannot simply be intuitively guessed, but may be obtained from the Open Quantum Materials Database (OQMD) [52], which contains over 280 000 DFT calculations of crystalline compounds at the time of this writing. The chemical potentials can be expressed in terms of a linear combination of the energies of these phases. The equilibrium states can be either two phase (MgB_2 and another phase) or three phase (MgB_2 and two other phases), depending on the topology of the Mg-B-TM ground state phase diagram. To illustrate this point, we show examples of TM = Sc and TM = Cu in Fig. 5. The $T = 0$ K phase diagram of Mg-B-Sc [Fig. 5(a)] indicates two reference states, since the dilutely Sc-doped MgB_2 lies on the tie line of MgB_2 and ScB_2. However, the phase diagram of Mg-B-Cu [Fig. 5(b)] gives a three-phase region as reference states, because the dilutely Cu-doped MgB_2 falls in the region of $MgCu_2$, MgB_2, and MgB_4. In the former case, only the chemical potential *difference* can be derived ($\mu_{Mg} - \mu_{TM} = E_{MgB_2} - E_{ScB_2}$). For the latter case, the chemical potentials of Cu, B, and Mg can be extracted by solving the linear equations $\mu_{Mg} + 2\mu_B = E_{MgB_2}$, $\mu_{Mg} + 4\mu_B = E_{MgB_4}$, and $\mu_{Mg} + 2\mu_{Cu} = E_{MgCu_2}$. We note that because we only consider TM substitution for Mg, we only need to know the chemical potential difference $\mu_{Mg} - \mu_{TM}$ [Eq. (3)]. Figure 6 shows the chemical difference ($\mu_{Mg} - \mu_{TM}$) and the formation energies of the reference states that contain

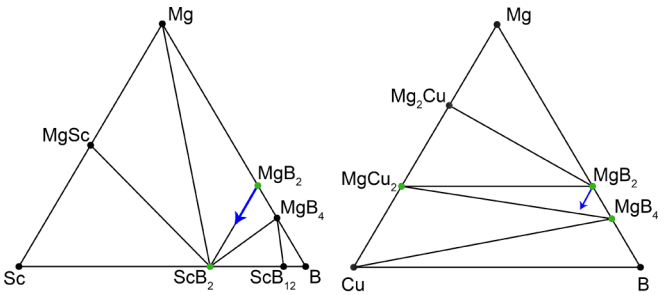

(a) Mg-B-Sc (b) Mg-B-Cu

FIG. 5. (Color online) Phase diagram of Mg-B-TM obtained from the Open Quantum Materials Database (OQMD) [52]. The reference states of the chemical potentials can be found in the three-phase region or two-phase tie line of the dilutely TM-doped MgB_2. The blue arrow indicates the doping direction. The green dots represent the reference states. MgB_2 is always one of the reference states. Figure 6 gives the formation energy of the second reference state. For Mn, Fe, Co, Ni, Cu, Zn, Ru, Rh, Pd, Ag, Cd, Pt, and Au systems, the third reference state is MgB_4. For Cr and Y systems, the third reference state is CrB and Mg, respectively. The rest systems only have two reference states. Further discussion can be found in Sec. III C.

TM atoms. The formation energy E_{form} is defined as the total energy difference between the reference state and ground states of composition elements (e.g., $E_{\text{form}}^{\text{ScB}_2} = E_{\text{DFT}}^{\text{ScB}_2} - E_{\text{DFT}}^{\text{Sc}} - 2E_{\text{DFT}}^{\text{Cu}}$). The reference states for the early transition metals are strongly bound compounds, while those for the late transition metals are more weakly bound. Correspondingly, the chemical potential for the early transition metals are generally stronger

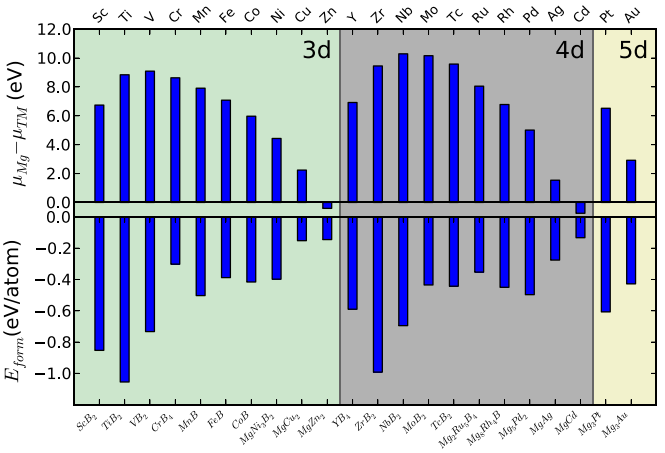

FIG. 6. (Color online) The chemical potentials of transition metals and the formation energies of the reference states that contain TM atoms. The reference-state sets are discussed in Sec. III C and also in the caption of Fig. 5. The bottom panel only shows the formation energies of the reference states that contain TM atoms. The formation energy E_{form} is defined as the total energy difference between the reference state and ground states of composition elements (e.g., $E_{\text{form}}^{\text{ScB}_2} = E_{\text{DFT}}^{\text{ScB}_2} - E_{\text{DFT}}^{\text{Sc}} - 2E_{\text{DFT}}^{\text{Cu}}$). The top panel presents the chemical potential difference Mg and TM, which is used in Eq. (3) to calculate the TM substitutional energy for one Mg on the MgB_2 surface.

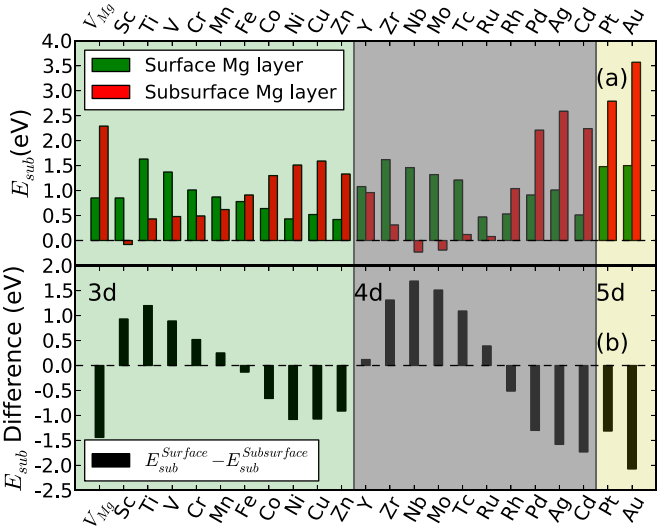

FIG. 7. (Color online) (a) The substitutional energies of Mg vacancy and transition metals on surface and subsurface sites of the Mg-terminated (0001) surface of MgB_2. The substitutional energy E_{sub} is defined in Eq. (3). Shown are E_{sub} for TMs doped in the surface and subsurface Mg layer. E_{sub} represents the required energy to substitute TM atom for Mg atom on MgB_2 surface. Positive E_{sub} indicates an endothermic doping process, while negative is exothermic. (b) The difference between substitutional energies of TMs doped in the surface and subsurface Mg layer. A negative value indicates that substituting in the surface Mg layer is more energetic favorable.

than those for late transition metals. Moreover, the chemical potentials for the 3*d* and 4*d* transition metals show a very similar pattern. The absolute value for the chemical potentials increase from Sc to V (3*d*) and from Y to Nb (4*d*), while gradually decrease from Cr to Zn (3*d*) and from Mo to Cd (4*d*).

The calculated E_{sub} values for various TMs, as well as those for the vacancy Mg at the surface and subsurface Mg layers, are illustrated in Fig. 7. A positive E_{sub} [Eq. (3)] value indicates the energy required to dope a TM from its bulk reference state on the MgB_2 surface. On the other hand, a negative E_{sub} indicates an exothermic doping process. The E_{sub} value for doping in the surface Mg layer generally decreases from Ti to Zn and from Zr to Cd, and from about 1.5 to 0.5 eV for both 3*d* and 4*d* transition metals. On the other hand, the E_{sub} value for doping in the subsurface Mg layer generally increases within each period. The energy difference between TM in the surface vs subsurface layers is also plotted in Fig. 7. According to the energy difference shown in Fig. 7, it is clear that late 3*d* and 4*d* transition metals prefer the surface Mg layer over the subsurface. Still the E_{sub} values are generally positive, and hence indicate an energy penalty that would need to be overcome to achieve significant TM concentration at the surface. The values of E_{sub} indicate the equilibrium thermodynamic solubility of TM at the surface is low. However, we note that it might be possible to achieve higher concentrations of TM on MgB_2 surfaces for kinetics reasons.

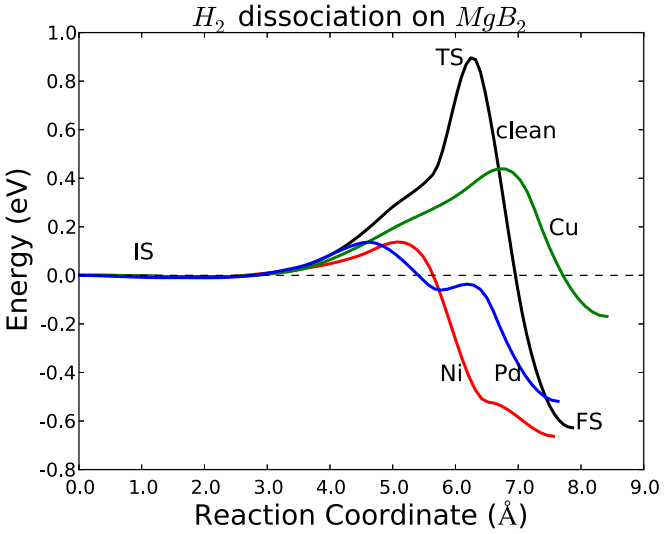

FIG. 8. (Color online) Minimum energy path for H_2 dissociation on the clean and Ni, Cu, and Pd-doped $MgB_2(0001)$ surface. IS, TS, and FS represent the initial, transition, and final states of hydrogen dissociation on the clean MgB_2 surface.

The energy required to create a Mg vacancy has a similar formula to Eq. (3), except that $E_{\text{slab}}^{\text{TM/MgB}_2}$ is the DFT total energy of MgB_2 slabs with one Mg vacancy at the surface and μ_{TM} is excluded. The reference states for μ_{Mg} and μ_{B} are the set of MgB_2 and MgB_4, because MgB_2 with dilute vacancies decomposes into these two phases in equilibrium. We find that the formation energy of an Mg vacancy is lowest in the surface layer, rather than in the subsurface layer, likely due to the fact that fewer bonds need to be broken at the surface.

D. H_2 dissociation and diffusion on the clean MgB_2 surface

Having investigated the hydrogen adsorption pattern on the MgB_2 in Sec. III B, we now turn to the discussion of hydrogen kinetic behaviors. In this section we focus on the clean Mg-terminated MgB_2 surface, and in the following section, TM-doped MgB_2 surfaces will be considered.

For the H_2 dissociation calculations, the initial state for the NEB calculation involves the hydrogen molecule positioned 5 Å away from the clean MgB_2 surface. Our DFT calculations find that the "binding energy" of a hydrogen molecule to the surface in this geometry is less than 6 meV/atom, which indicates that this 5 Å distance is large enough to approximate complete separation. Since it is one hydrogen molecule dissociated on a 2×2 surface unit cell, the coverage ratio for the dissociated state (the final state for the NEB calculations) will be 0.5 ML. As discussed in Sec. III B, the most stable adsorption pattern found for 0.5 ML on the 2×2 surface unit cell is shown in Fig. 4(a). We explore the minimum energy pathway of hydrogen dissociating on the clean Mg-terminated $MgB_2(0001)$ surface using the pattern shown in Fig. 4(a) as the final image.

Using nine intermediate images between the initial state and the final state, the NEB calculations identify a 0.89 eV dissociation barrier for H_2 on the $MgB_2(0001)$ surface. Figure 8 illustrates the initial state (IS), transition state (TS), and final state (FS) for hydrogen molecular dissociation. At the transition state, the hydrogen atoms are separated by 1.38 Å and are 1.40 Å above the surface Mg layer. We observed that from 5.00 to 1.90 Å above the surface Mg layer, the two hydrogen atoms stay in the molecular state, with bond length increasing less than 0.05 Å from the original molecular value of 0.74 Å.

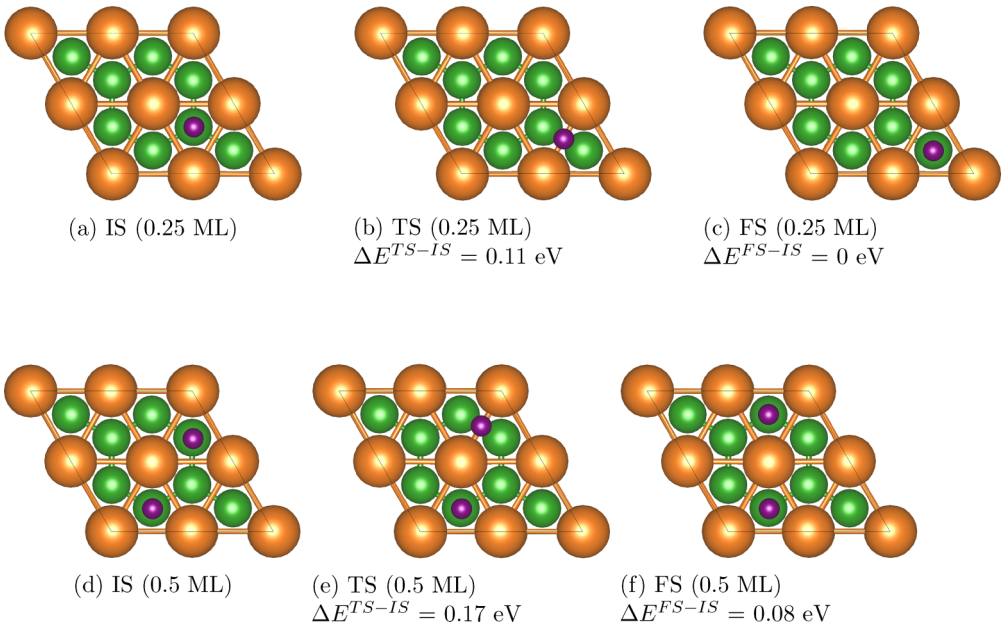

FIG. 9. (Color online) H diffusion on the MgB_2 surface as viewed from the top. From left to right, subfigures show hydrogen positions at IS, TS, and FS. The top panel shows the hydrogen diffusion under 0.25 ML hydrogen coverage, while the bottom panel are under 0.5 ML coverage. The Mg, B, and H atoms are represented by orange, green, and purple, respectively.

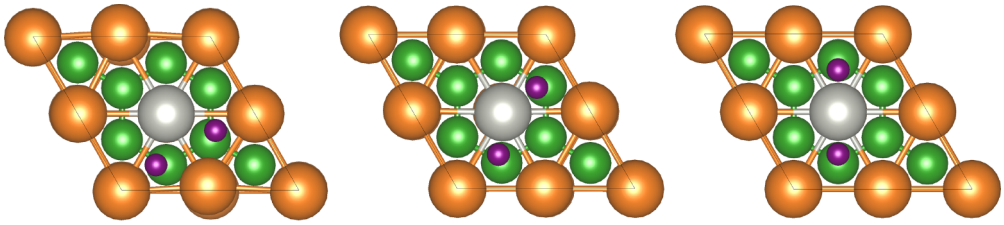

FIG. 10. (Color online) The three kinds of hydrogen dissociation geometries on the TM-doped MgB_2 surface we investigated. The three geometries are named as pattern 1, pattern 2, and pattern 3, respectively. The figures shown here are the top view of the relaxed TM-doped MgB_2 surface with the purple, green, orange, and gray atoms representing the H, B, Mg, and TM species.

After H_2 dissociates, the diffusion of the resulting adsorbed H atoms is also another important kinetic barrier that we address. Regarding atomic hydrogen diffusion on the Mg-terminated $MgB_2(0001)$ surface, we considered the following two cases: (1) diffusion of a single atomic hydrogen within the 2×2 unit cell (0.25 ML) and (2) one atomic hydrogen diffuses within the 2×2 unit cell, with a second hydrogen atom fixed (0.5 ML). Figures 9(a)–9(c) illustrate the first case. The transition state is only 0.11 eV higher than the initial state in Fig. 9, while the initial state and the final state energies are equal. The low diffusion barrier at the 0.25 ML coverage indicates facile hydrogen movement from one hollow site passing through a bridge site to a nearby hollow site. We also show the hydrogen diffusion pathway for the 0.5 ML coverage ratio in Figs. 9(d)–9(f). The IS and FS in Fig. 9 correspond to the adsorption configuration of 0.5 ML coverage ratio shown in Figs. 4(a) and 4(b). For the second case, our NEB calculations found a slightly higher migration energy of 0.17 eV from IS to FS. This increase of 0.06 eV in migration energy is simply due to the fact that the FS is around 0.06 eV higher than the IS. Still, the migration barrier at 0.5 ML coverage is quite low.

It is interesting that our results on the Mg-terminated MgB_2 surface have a qualitative similarity with that on the pure Mg surface: high dissociation barrier and low diffusion barrier. Vegge [34] applied NEB with DFT calculations to find a 1.15 eV dissociation barrier for H_2 on the Mg surface. He also found [34] a low diffusion barrier of 0.15 eV for atomic H from one fcc to another fcc site. Other computations of the interaction between hydrogen and Mg surfaces [29,60] also predicted a low barrier for hydrogen diffusion, which are less than 0.2 eV.

In this section we found a H_2 dissociation barrier on the Mg-terminated $MgB_2(0001)$ surface of 0.89 eV, which indicates a possible rate limiting step for rehydrogenation. The hydrogen diffusion barrier is less than 0.2 eV, indicating a fast migration at room temperature. The almost barrierless diffusion of dissociated H atoms are also observed in the previous studies [61,62]. In the following section we will discuss the effects of surface transition metals on H_2/H behavior.

E. H_2 dissociation and diffusion on TM-doped MgB_2 surfaces

We now investigate the effects of the transition metal dopants on the hydrogen dissociation and diffusion barriers on the MgB_2 surface. First, the adsorption geometry of atomic H on the TM-doped surface requires further investigation. Three kinds of adsorption patterns are explored (Fig. 10). The hydrogen binding energies of the three relaxed adsorption patterns are shown in Fig. 11, and for the majority of the transition metals, the stable adsorption geometry is pattern 3. Without the TM, pattern 2 is preferred, so the presence of the TM changes the preferred H adsorption geometry. We note that the hydrogen adsorption geometry for Cu, Zn, Cd, and Au does not adopt pattern 3. Figure 12 presents the most stable pattern we found for Cu, Zn, Cd, and Au doped surfaces. In both of these geometries, one or more of the H atoms bind in hollow sites surrounded entirely by Mg (i.e., they do not bind to the TM). Interestingly, for these metals there is no stable Cu, Zn, Cd, or Au hydride, and no stable ternary Mg-TM-H hydrides. Therefore, it is reasonable that the adsorbed hydrogen would prefer binding with Mg to Cu/Zn/Cd/Au. For each of our calculations of the two atomic hydrogens adsorbed on the TM-doped Mg-terminated $MgB_2(0001)$ surfaces with 2×2 unit cells, the most stable adsorption pattern will be used as the final image in the following NEB studies of dissociation.

The activation barriers for H_2 dissociation over the various transition metal doped MgB_2 surfaces are reported in Fig. 13 and Table II. The Ag-doped MgB_2 surface shows the largest

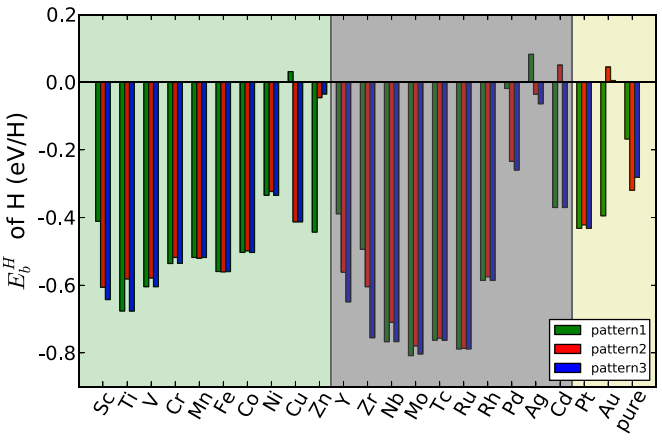

FIG. 11. (Color online) Binding energy of atomic hydrogen on the various transition metal doped Mg-terminated $MgB_2(0001)$ surfaces. The binding energy has a similar definition to Eq. (2), where a negative value indicates the atomic hydrogen is energetically bound on the surface. Patterns 1, 2, and 3 in the legend refer to the three kinds of hydrogen dissociation geometries on the TM-doped MgB_2 surface we investigated, as shown in Fig. 10.

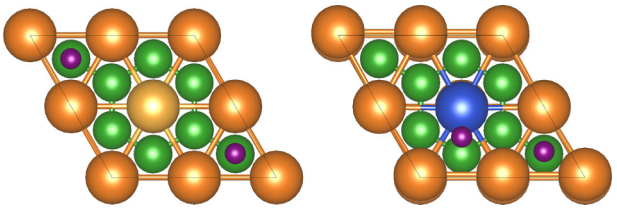

FIG. 12. (Color online) The stable adsorption pattern for Zn, Cd, Au (left figure), and Cu (right figure). These patterns are obtained from DFT relaxation, with the input structures of pattern 3 [Fig. 10(c)].

activation barrier among all the dopants we investigated. Cd and Au doped surfaces also have a larger barrier than on the clean MgB_2 surface. For these dopants, H_2 will not preferentially dissociate onto Ag, Cd, and Au sites, but could more easily dissociate on regions of the Mg layer free of the dopants. On the other hand, the early transition metals provide a strong effect on the dissociation of H_2 molecule. Sc, Ti, Zr, and Nb doped surfaces have dissociation barriers almost exactly equal to zero. Incidentally, these four elements also possess strongly bound, stable hydride phases. In general, most of the transition metal dopants on the MgB_2 surface reduce or even eliminate the dissociation barrier, except Ag, Cd, and Au (elements with no stable hydrides).

Following dissociation, the next fundamental step is the diffusion of atomic hydrogen away from the dopant catalytic sites. Figure 14 shows the diffusion path of one of the two hydrogen atoms on the Pd-doped MgB_2 surface as an example. The diffusion and dissociation barriers are shown in Table II. For many TM, the energy barriers of dissociation and diffusion exhibit an inverse correlation (Fig. 15). That is, if a transition metal reduces the dissociation barrier, it often increases the diffusion barrier, and vice versa. This correlation is reasonable, since one might expect that a transition metal dopant which strongly reduces the dissociation barrier may also result in a strong TM-H binding energy, which prevents fast hydrogen diffusion. In fact, Sc, Ti, Zr, and Nb have essentially zero dissociation barriers, but they bind the atomic

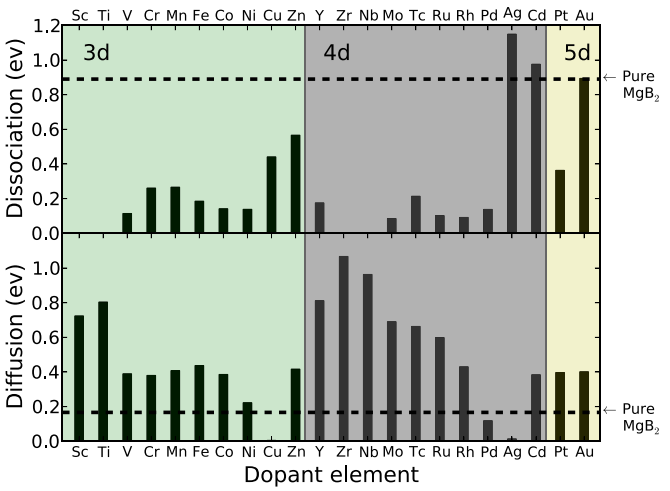

FIG. 13. (Color online) The dissociation and diffusion barriers of hydrogen on the TM-doped Mg-terminated MgB_2(0001) surface.

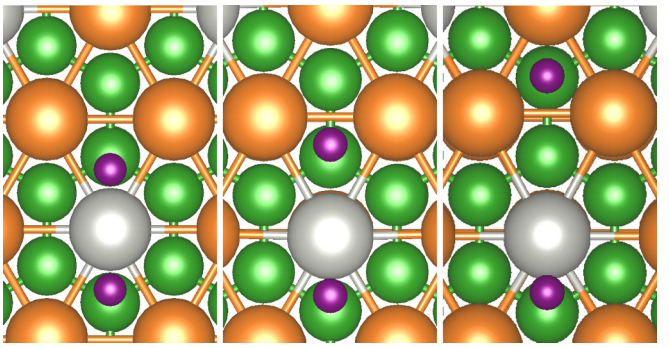

FIG. 14. (Color online) H diffusion on the Pd-doped MgB_2 surface. From left to right, subfigures show hydrogen positions at IS, TS, and FS. The Mg, B, Pd, and H atoms are represented by orange, green, gray, and purple, respectively.

H very strongly, which results in high values of E_{diff}. Such high surface diffusion barriers reduce hydrogen mobility and potentially localize atomic hydrogen around early transition metal dopants, which could then further reduce the TM ability of dissociating further H_2 molecules. On the other hand, Ag, Cd, and Au give rise to large dissociation barriers, but they have low diffusion barriers, and there is no diffusion barrier at all for Ag. Between these two extremes, V, Cr, Mn, Fe, and Co present a compromised combination of the dissociation and diffusion barriers. V, Cr, Mn, Fe, and Co as dopants can

TABLE II. The energy barrier for the dissociation of H_2 (E_{diss}), the energy difference between the final and initial state (E_{diss}^{FS-IS}) of the dissociation, the migration barrier for the diffusion of atomic H (E_{diff}), and the corresponding energy difference (E_{diff}^{FS-IS}) on the clean Mg-terminated MgB_2(0001) surface as well as on the transition metal doped MgB_2 surfaces (unit: eV).

Surface	E_{diss}	E_{diss}^{FS-IS}	E_{diff}	E_{diff}^{FS-IS}
Clean	0.89	−0.63	0.17	0.08
Sc doped	0.00	−1.28	0.72	0.72
Ti doped	0.00	−1.34	0.80	0.80
V doped	0.11	−1.20	0.39	0.33
Cr doped	0.26	−1.07	0.38	0.19
Mn doped	0.27	−1.03	0.41	0.08
Fe doped	0.18	−1.12	0.44	0.10
Co doped	0.14	−1.01	0.39	−0.02
Ni doped	0.14	−0.66	0.22	−0.34
Cu doped	0.44	−0.17	0.00	−0.65
Zn doped	0.57	−0.88	0.42	0.37
Y doped	0.17	−1.29	0.81	0.81
Zr doped	0.00	−1.50	1.07	1.07
Nb doped	0.00	−1.53	0.96	0.96
Mo doped	0.08	−1.60	0.69	0.69
Tc doped	0.21	−1.52	0.66	0.58
Ru doped	0.10	−1.57	0.60	0.53
Rh doped	0.09	−1.17	0.43	0.22
Pd doped	0.14	−0.52	0.12	−0.30
Ag doped	1.15	−0.12	0.01	−0.44
Cd doped	0.98	−0.74	0.38	0.00
Pt doped	0.36	−0.86	0.40	−0.20
Au doped	0.89	−0.79	0.40	0.00

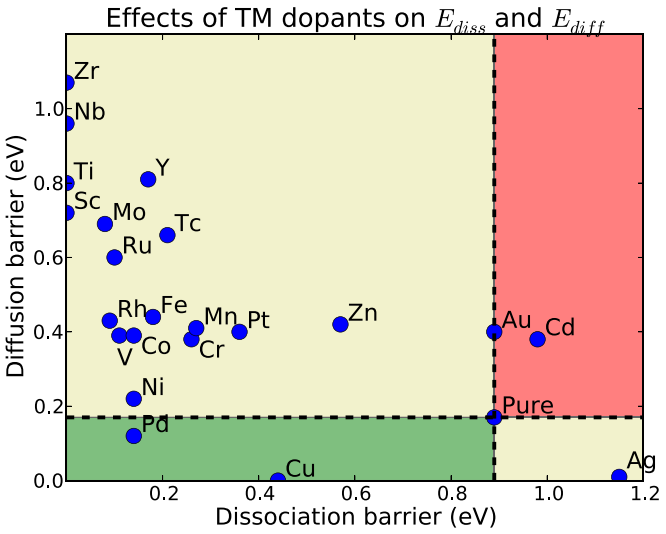

FIG. 15. (Color online) H_2 dissociation vs H diffusion barriers on pure and TM-doped Mg-terminated $MgB_2(0001)$ surface. The green area indicates TM dopants that reduce both pure (undoped) surface dissociation and diffusion barriers. The light yellow area represents TM dopants that reduce only dissociation or diffusion barriers, but simultaneously increase the other barrier. TM dopants that fall in the red area increase both dissociation and diffusion barriers. The promising catalytic dopants should be in or near the green area, close to the origin. Pd and Cu as dopants can reduce both dissociation and diffusion barriers. Ni dopants reduce the dissociation barrier without significantly increasing the diffusion barrier. Therefore, Pd, Cu, and Ni are promising catalytic dopants.

reduce dissociation barrier by 0.6–0.7 eV, without significantly increasing the diffusion barrier (around 0.2 eV or less). Over all of the studied transition metals, Ni, Cu, and Pd give the best catalytic effect on dissociation and diffusion. Ni reduces the dissociation barrier from 0.89 eV on the clean MgB_2 surface to 0.14 eV, while only slightly increasing the diffusion barrier to 0.22 eV. Pd reduces the activation barriers for both the processes to 0.14 and 0.12 eV. With essentially zero diffusion barrier, Cu provides a 0.44 eV dissociation barrier.

As a final note, we also observe several interesting similarities between the TM-doped MgB_2 surface and TM-doped Mg surface. Using DFT, Du *et al.* [40] identify an almost zero hydrogen dissociation barrier on Ti-doped Mg(0001) surface, but also found the dissociated hydrogen bind strongly to the Ti dopant. In another first-principle study, Pozzo and co-workers [30,39] found a 1.18 eV dissociation barrier for Ag-doped Mg surface, and moderate dissociation barriers for Ni(0.06 eV), Cu(0.56 eV), and Pd(0.39 eV) doped surfaces. Jensen *et al.* [63] experimentally demonstrated the catalytic effect of Ni dopant on Mg surfaces for the dehydrogenation process, showing an activation energy reduced by 0.5 eV with respect to that on the clean Mg surface.

IV. CONCLUSIONS

We have presented a systematic DFT/GGA study of hydrogen adsorption, dissociation, and subsequent diffusion on the MgB_2 surface with and without various transition metals. After considering the surface energies of Mg-terminated (0001), $(10\bar{1}0)$, B-terminated (0001), $(10\bar{1}0)$, and Mg-B-terminated $(11\bar{2}0)$ MgB_2 surfaces, we found the Mg-terminated MgB_2 (0001) has the lowest surface energy (less than 1.3 J/m^2). Therefore, we used this Mg-terminated $MgB_2(0001)$ surface as our reference surface to study the interaction with hydrogen molecules and atoms. We investigated the stable hydrogen adsorption configuration under coverage ratios from 1/9 to 2 ML on 1×1, 2×2, and 3×3 unit cells. Though the adsorbed H–H interaction is repulsive, the absolute value of hydrogen binding energy increases with respect to coverage ratio up to 1 ML. We studied hydrogen dissociation and diffusion on the clean MgB_2 surface, and we identified a dissociation barrier of 0.89 eV and a diffusion barrier of 0.17 eV. The activation barriers suggested a sluggish H_2 dissociation but a fast atomic hydrogen movement on the surface. Next, we consider the role of transition metal on the dissociation and diffusion processes. Based on the substitutional energy of one transitional metal species with one Mg atom, we found that the late transition metals is more energetically favorable to dope on the surface Mg layer than the subsurface Mg layer, but that the equilibrium solubility of dopants is very small. We examined three possible hydrogen adsorption configurations on the TM-doped MgB_2 surface, and found in contrast to the clean surface, the two adsorbed atomic hydrogen would bind with transition metal dopant while maximizing the H-H distance. Except for Ag, Cd, and Au, the transition metals that we studied can always reduce the dissociation barrier, but most of them also increase the diffusion barrier. Sc, Ti, Zr, and Nb doped surfaces have null dissociation barrier, but they bind with adsorbed hydrogen very strongly, limiting the consequent hydrogen diffusion process. On the other hand, V, Cr, Mn, Fe, and Co can reduce the dissociation barrier to around 0.2 eV, without increasing the diffusion barrier above 0.4 eV. Similar to the situation on the Mg(0001) surface, Ni, Cu, and Pd show promise as catalytic dopants, successfully decreasing the dissociation barrier and keeping the diffusion barrier at acceptable level.

ACKNOWLEDGMENTS

Y.W. gratefully acknowledges financial support from the US Department of Energy under Grant No. DE-FC36-08GO18136. K.M., Y.Z. and C.W. gratefully acknowledge financial support from the US Department of Energy under Grant No. DE-FG02-07ER46433. This research used the resources of the National Energy Research Scientific Computing Center, which is supported by the Office of Science of the US Department of Energy under Contract No. DE-AC02-05CH11231.

[1] S.-i. Orimo, Y. Nakamori, J. R. Eliseo, A. Züttel, and C. M. Jensen, Chem. Rev. **107**, 4111 (2007).

[2] J. Yang, A. Sudik, C. Wolverton, and D. J. Siegel, Chem. Soc. Rev. **39**, 656 (2010).

[3] H.-W. Li, Y. Yan, S.-i. Orimo, A. Züttel, and C. M. Jensen, Energies **4**, 185 (2011).

[4] J. J. Vajo, Current Opinion Solid State Mater. Sci. **15**, 52 (2011).

[5] C. Wolverton, D. J. Siegel, A. R. Akbarzadeh, and V. Ozolins, J. Phys.: Condens. Matter **20**, 064228 (2008).

[6] G. Walker, *Solid-State Hydrogen Storage: Materials and Chemistry* (CRC Press, Boca Raton, FL, 2008).

[7] D. P. Broom, *Hydrogen Storage Materials: The Characterisation of Their Storage Properties* (Springer, New York, 2011).

[8] DOE Targets for Onboard Hydrogen Storage Systems for Light-Duty Vehicles. http://www1.eere.energy.gov/hydrogenandfuelcells/storage/pdfs/targets_onboard_hydro_storage.pdf (2010).

[9] B. Bogdanovic and M. Schwickardi, J. Alloys Compounds **253–254**, 1 (1997).

[10] D. J. Siegel, C. Wolverton, and V. Ozoliņš, Phys. Rev. B **76**, 134102 (2007).

[11] Y. Wang, Y. Zhang, and C. Wolverton, Phys. Rev. B **88**, 024119 (2013).

[12] A. R. Akbarzadeh, V. Ozoliņš, and C. Wolverton, Adv. Mater. **19**, 3233 (2007).

[13] 14.9% H_2 by weight is the "material-only" hydrogen storage capacity. The targeted ranges set by DOE are "system level" and would have to account for all balance of plant considerations.

[14] H.-W. Li, K. Kikuchi, Y. Nakamori, K. Miwa, S. Towata, and S. Orimo, Scr. Mater. **57**, 679 (2007).

[15] G. L. Soloveichik, Y. Gao, J. Rijssenbeek, M. Andrus, S. Kniajanski, R. C. Bowman Jr., S.-J. Hwang, and J.-C. Zhao, Int. J. Hydrogen Energy **34**, 916 (2009).

[16] B. Dai, D. S. Sholl, and J. K. Johnson, J. Phys. Chem. C **112**, 4391 (2008).

[17] T. Matsunaga, F. Buchter, P. Mauron, M. Bielman, Y. Nakamori, S. Orimo, N. Ohba, K. Miwa, S. Towata, and A. Züttel, J. Alloys Compounds **459**, 583 (2008).

[18] V. Ozoliņš, E. H. Majzoub, and C. Wolverton, J. Am. Chem. Soc. **131**, 230 (2009).

[19] V. Ozoliņš, E. H. Majzoub, and C. Wolverton, Phys. Rev. Lett. **100**, 135501 (2008).

[20] Y. Zhang, E. Majzoub, V. Ozoliņš, and C. Wolverton, Phys. Rev. B **82**, 174107 (2010).

[21] Y. Zhang, E. Majzoub, V. Ozoliņš, and C. Wolverton, J. Phys. Chem. C **116**, 10522 (2012).

[22] N. Hanada, K. Chlopek, C. Frommen, W. Lohstroh, and M. Fichtner, J. Mater. Chem. **18**, 2611 (2008).

[23] G. Severa, E. Ronnebro, and C. M. Jensen, Chem. Commun. **46**, 421 (2010).

[24] J. J. Vajo, S. L. Skeith, and F. Mertens, J. Phys. Chem. B **109**, 3719 (2005).

[25] J. J. Vajo, W. Li, and P. Liu, Chem. Commun. **46**, 6687 (2010).

[26] R. J. Newhouse, V. Stavila, S.-J. Hwang, L. E. Klebanoff, and J. Z. Zhang, J. Phys. Chem. C **114**, 5224 (2010).

[27] Y. Wang, F. Zhang, R. Stumpf, P. Lin, and M. Y. Chou, Phys. Rev. B **83**, 195419 (2011).

[28] F. Zhang, Y. Wang, and M. Y. Chou, J. Phys. Chem. C **116**, 18663 (2012).

[29] A. J. Du, S. C. Smith, X. D. Yao, and G. Q. Lu, J. Am. Chem. Soc. **129**, 10201 (2007).

[30] M. Pozzo and D. Alfé, Int. J. Hydrogen Energy **34**, 1922 (2009).

[31] B. Dai, D. S. Sholl, and J. K. Johnson, J. Phys. Chem. C **111**, 6910 (2007).

[32] A. Du, S. C. Smith, X. Yao, and G. Lu, Surf. Sci. **600**, 1854 (2006).

[33] S. Hao and D. S. Sholl, Appl. Phys. Lett. **94**, 171909 (2009).

[34] T. Vegge, Phys. Rev. B **70**, 035412 (2004).

[35] K. J. Michel, Y. Zhang, and C. Wolverton, J. Phys. Chem. C **117**, 19295 (2013).

[36] S. Hao and D. S. Sholl, J. Phys. Chem. Lett. **1**, 2968 (2010).

[37] K. C. Kim, B. Dai, J. K. Johnson, and D. S. Sholl, Nanotechnology **20**, 204001 (2009).

[38] M. Pozzo and D. Alfè, Phys. Rev. B **78**, 245313 (2008).

[39] M. Pozzo, D. Alfe, A. Amieiro, S. French, and A. Pratt, J. Chem. Phys. **128**, 094703 (2008).

[40] A. J. Du, S. C. Smith, X. D. Yao, and G. Q. Lu, J. Phys. Chem. B **110**, 21747 (2006).

[41] Y. Wang, K. Michel, and C. Wolverton (unpublished).

[42] P. Hohenberg and W. Kohn, Phys. Rev. **136**, B864 (1964).

[43] W. Kohn and L. J. Sham, Phys. Rev. **140**, A1133 (1965).

[44] G. Kresse and J. Furthmüller, Phys. Rev. B **54**, 11169 (1996).

[45] J. P. Perdew, J. A. Chevary, S. H. Vosko, K. A. Jackson, M. R. Pederson, D. J. Singh, and C. Fiolhais, Phys. Rev. B **46**, 6671 (1992).

[46] P. E. Blöchl, Phys. Rev. B **50**, 17953 (1994).

[47] G. Kresse and D. Joubert, Phys. Rev. B **59**, 1758 (1999).

[48] B. Berne, G. Ciccotti, and D. Coker, *Classical and Quantum Dynamics in Condensed Phase Simulations: Proceedings of the International School of Physics "Computer Simulation of Rare Events and the Dynamics of Classical and Quantum Condensed-Phase Systems"* (World Scientific, Singapore, 1998).

[49] S. Ganeshan, L. G. Hector Jr., and Z.-K. Liu, Acta Mater. **59**, 3214 (2011).

[50] G. Henkelman, B. P. Uberuaga, and H. Jonsson, J. Chem. Phys. **113**, 9901 (2000).

[51] M. E. Jones and R. E. Marsh, J. Am. Chem. Soc. **76**, 1434 (1954).

[52] J. Saal, S. Kirklin, M. Aykol, B. Meredig, and C. Wolverton, JOM **65**, 1501 (2013).

[53] G. Profeta, A. Continenza, F. Bernardini, and S. Massidda, Phys. Rev. B **66**, 184517 (2002).

[54] V. D. P. Servedio, S.-L. Drechsler, and T. Mishonov, Phys. Rev. B **66**, 140502 (2002).

[55] I. G. Kim, J. I. Lee, B. I. Min, and A. J. Freeman, Phys. Rev. B **64**, 020508 (2001).

[56] V. M. Silkin, E. V. Chulkov, and P. M. Echenique, Phys. Rev. B **64**, 172512 (2001).

[57] Y. Zhang, V. Blum, and K. Reuter, Phys. Rev. B **75**, 235406 (2007).

[58] D. J. Schmidt, W. Chen, C. Wolverton, and W. F. Schneider, J. Chem. Theory Comput. **8**, 264 (2012).

[59] D. J. Siegel, L. G. Hector Jr., and J. B. Adams, Surf. Sci. **498**, 321 (2002).

[60] N. Jacobson, B. Tegner, E. Schrder, P. Hyldgaard, and B. Lundqvist, Comput. Mater. Sci. **24**, 273 (2002).

[61] P. Abanador, A. C. Villagracia, and J. N. B. Arboleda, Phillippine Sci. Lett. **6**, 176 (2013).

[62] A. J. Du, S. C. Smith, X. D. Yao, C. H. Sun, L. Li, and G. Q. Lu, J. Nanosci. Nanotech. **9**, 4388 (2009).

[63] T. R. Jensen, A. Andreasen, T. Vegge, J. W. Andreasen, K. Ståhl, A. S. Pedersen, M. M. Nielsen, A. M. Molenbroek, and F. Besenbacher, Int. J. Hydrogen Energy **31**, 2052 (2006).